JMEPEG (2012) 21:2–16
DOI: 10.1007/s11665-011-9875-6

1059-9495/$19.00

Experimental Characterization and Material-Model Development for Microphase-Segregated Polyurea: An Overview

M. Grujicic, T. He, B. Pandurangan, F.R. Svingala, G.S. Settles, and M.J. Hargather

(Submitted December 17, 2010)

Numerous experimental investigations reported in the open literature over the past decade have clearly demonstrated that the use of polyurea external coatings and/or inner layers can substantially enhance both the blast resistance (the ability to withstand shock loading) and the ballistic performance (the ability to defeat various high-velocity projectiles such as bullets, fragments, shrapnel, etc. without penetration, excessive deflection or spalling) of buildings, vehicles, combat-helmets, etc. It is also well established that the observed high-performance of polyurea is closely related to its highly complex submicron scale phase-segregated microstructure and the associated microscale phenomena and processes (e.g., viscous energy dissipation at the internal phase boundaries). As higher and higher demands are placed on blast/ballistic survivability of the foregoing structures, a need for the use of the appropriate transient nonlinear dynamics computational analyses and the corresponding design-optimization methods has become ever apparent. A critical aspect of the tools used in these analyses and methods is the availability of an appropriate physically based, high-fidelity material model for polyurea. There are presently several public domain and highly diverse material models for polyurea. In the present work, an attempt is made to critically assess these models as well as the experimental methods and results used in the process of their formulation. Since these models are developed for use in the high-rate loading regime, they are employed in the present work, to generate the appropriate shock-Hugoniot relations. These relations are subsequently compared with their experimental counterparts in order to assess the fidelity of these models.

Keywords experimental characterization, material-model development, microphase-segregated polyurea

1. Introduction

Polyurea is a microphase-segregated and thermo-plastically linked elastomeric copolymer (the terms ''microphase-segregated'' and ''thermoplastically linked'' will be explained later) that is formed by the rapid chemical reaction between an isocyanate (an organic chemical containing isocyanate –N=C=O group) and an amine (organic chemical containing amine $–NH_2$ group). A schematic of the polyurea copolymerization reaction is shown in Fig. 1, in which symbol R is used to represent an aromatic functional group (e.g., di-phenyl methane), while R' is used to denote an aromatic/aliphatic long chain functional group (e.g., polytetramethyleneoxide-di-phenyl). Since the copolymerization/gel reaction times are typically less than a minute, polyurea synthesis can be achieved under a wide range of temperatures and humidity without significantly affecting material microstructure and properties.

M. Grujicic, T. He, and **B. Pandurangan**, Department of Mechanical Engineering, Clemson University, 241 Engineering Innovation Building, Clemson, SC 29634-0921; and **F.R. Svingala, G.S. Settles,** and **M.J. Hargather**, Department of Mechanical Engineering, Pennsylvania State University, University Park, PA 16082. Contact e-mail: gmica@clemson.edu.

As seen in Fig. 1, the copolymerization reaction creates urea linkages which are highly polar, i.e., contain centers/poles of negative and positive charge. Also shown in Fig. 1 is that urea linkages together with the R functional groups form the so-called ''hard segments'' within individual polyurea chains. Within the same chains, R' functional groups form the so-called ''soft segments.'' As a result of strong hydrogen bonding between urea linkages of the neighboring chains (or the neighboring portions of the same chain), hard segments are typically microphase segregated into the so-called ''hard domains.'' An example of the formation of hard domains within polyurea is shown in Fig. 2 using a tapping-mode atomic force micrograph. As shown in this figure [high-glass transition temperature (T_g) and crystallizable (Ref 1)] hard domains are present as isolated rod-like entities within the compliant/soft (i.e., low-glass transition temperature, T_g) matrix composed of nonphase-segregated hard segments and soft segments. In some cases, hard domains are interconnected forming a contiguous network. Since hydrogen bonding within hard domains provides interchain joining, polyureas are often referred to as being thermo-plastically crosslinked (in contrast to more commonly covalently crosslinked thermosetting) polymers. Thus, hard domains within polyurea act both as stiff/strong reinforcements and also as interchain links. Based on the aforementioned molecular- and domain-level microstructures, polyurea is usually described as a microphase-segregated and thermo-plastically crosslinked elastomer (or nanoscale elastomer-based composite).

Due to their highly complex internal microstructure described above, polyurea displays a very broad range of

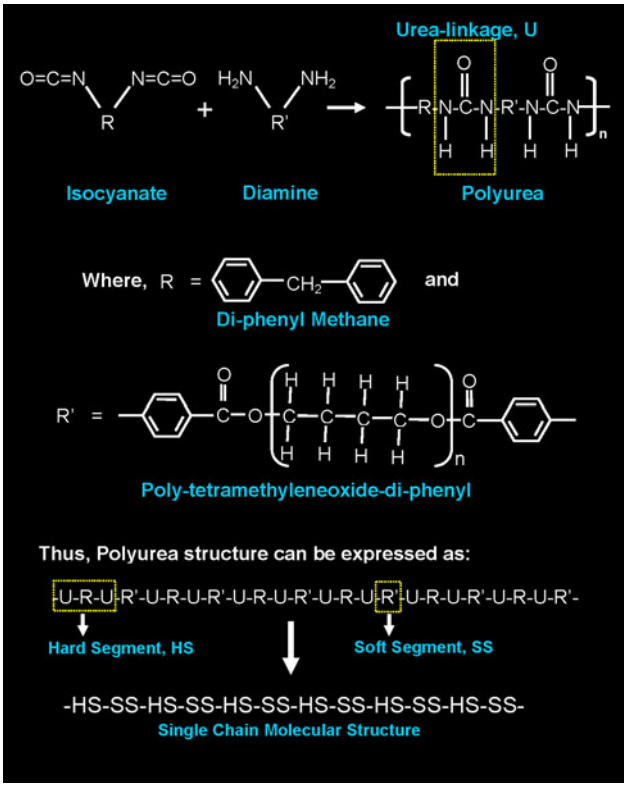

Fig. 1 Copolymerization reaction resulting in the formation of segmented polyurea. To simplify the schematic of the molecular structure, symbols HS (hard segment) and SS (soft segment) are used

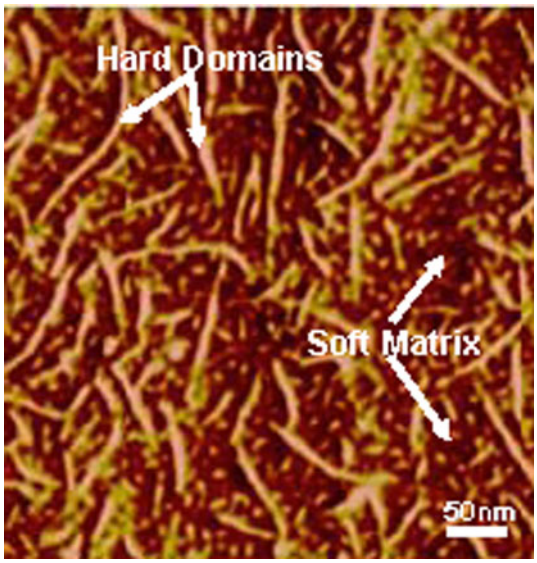

Fig. 2 An example of a typical tapping-mode AFM image of a polyurea showing a rod-like morphology of the hard segments

mechanical responses under dynamic-loading conditions. The main features of this response can be defined as: (a) a high-level of stress versus strain constitutive nonlinearity; (b) extreme strain-rate (and temperature) sensitivity; and (c) a high degree of pressure dependence. A more detailed description of the mechanical response of polyurea when subjected to different quasi-static and dynamic deformation modes is provided in the subsequent section of this manuscript.

Polyurea has been used commercially for more than a decade. The most common applications of polyurea include:

(a) Tough, abrasion-resistant, corrosion-resistant, durable and impact-resistant (epoxy/rubber replacement) spray-on coatings/liners in various construction/structural applications such as tunnels, bridges, roofs, parking decks, storage tanks, freight ships, truck beds, etc.;
(b) External and internal wall-sidings and foundation coatings for buildings aimed at minimizing the degree of structure fragmentation and, in turn, minimizing the extent of the associated collateral damage in the case of a bomb blast; and
(c) Gunfire/ballistic resistant and explosion/blast mitigating coatings/liners or interlayers in blast-resistant sandwich panels for military vehicles and structures.

In light of the aforementioned growing applications of polyurea in blast-mitigation and impact-protection applications, there has been substantial effort over the last few years to characterize the mechanical response of polyurea under a wide range of strain rates including high-speed loading conditions. The main outcomes of this effort are summarized in the next section. It is generally observed that the mechanical response of polyurea is quite complex and that it is the result of the competition and interaction of a number of processes/mechanisms. Among these, the ones making the dominant contribution to the mechanical response of this class of elastomers are:

(a) Rate/time independent (equilibrium) hyperelastic (HE) behavior which dominates material mechanical response at low-strain rates;
(b) Large-strain material degradation which results in a more compliant behavior of the predeformed material;
(c) Rate/time-dependent visco-plastic material behavior which dominates material mechanical response at the intermediate- and high-strain rates. It should be noted that at extremely high-strain rates, the material mechanical response may become again effectively rate/time independent. However, due to fully unrelaxed state of the material in this case, materials' stiffness will be substantially higher than that observed in the equilibrium state; and
(d) When subjected to blast and impact loading conditions, the resulting high-pressure conditions can significantly affect both the equilibrium hyper-elastic and the finite-rate visco-plastic material response.

The applications of polyurea mentioned above capitalize on the exceptional ability of polyurea to alter/disperse shock waves and to absorb the kinetic energy associated with these waves (Ref 2) under high-rate loads (Ref 3). This shock-dispersion/energy-absorption has been linked to its ability to undergo a deformation-induced phase transition during which the rubbery state of the material is converted to the glassy state (Ref 4).

The development of the aforementioned blast/ballistic-protection systems based on the use of polyurea typically involves an extensive use of experimental test programs. Such experimental programs are critical for ensuring the utility and effectiveness of these protection systems. However, the use of the experimental programs is generally expensive, time-consuming, involves damage to or destruction of the test structures. Hence, the development of these protective systems

using solely the fabricate and test approaches is often cost prohibitive. It is hence no surprise that, while the utility of experimental test programs remains recognized, they are increasingly being complemented with the corresponding computation-based engineering analyses and simulations. Recent advances in numerical analysis capabilities, particularly the coupling of Eulerian solvers (used to model gaseous detonation products and air) and Lagrangian solvers (used to represent protective systems/test structures), have enabled quite realistic computational simulations of various blast/ballistic-impact loading conditions/scenarios. Nevertheless, the computer engineering analyses in question have to be characterized as not being fully mature. As discussed in our previous work (Ref 5-15), the lack of maturity of computer simulations of the blast/ballistic-impact events is mainly a consequence of inability of the present material models (including the one for polyurea) to realistically represent the response of the materials subjected to large-deformation, high-deformation rate, high-pressure conditions (the type of loading conditions encountered under different blast/ballistic-impact events).

The main objective of the present work is to conduct a critical assessment of all the publically available material models for polyurea and of all the experimental methods and tools used to obtain data needed during the formulation of these models. In addition, an attempt is made to test the validity/fidelity of these models by comparing their shock-Hugoniot predictions with the available experimental results.

The organization of the article is as follows. A brief overview of the main experimental efforts reported in the open literature pertaining to the characterization of the mechanical response of polyurea under various quasi-static and dynamic deformation modes is presented in section 2. A critical assessment of the material mechanical models for polyurea reported in the open literature is presented in section 3. The procedures used to generate the shock Hugoniots from the computational results obtained in a slug-impact analysis are discussed in section 4. The main conclusions resulting from the present work are summarized in section 5.

2. Overview of the Prior Experimental Investigations

In this section, a brief overview is presented of the main findings pertaining to the experimental investigations, reported in the open literature, of the deformation behavior of polyurea under different quasi-static and dynamic-loading conditions. It should be noted that the overview includes only the experimental studies which were focused on generating the data used in the polyurea material-model derivation process. In other words, a vast body of experimental studies pertaining to the blast/ballistic-protection performance of various polyurea bearing protective structures was not the subject of the present investigation. An overview of the latter investigations can be found in our prior work (Ref 16-21).

The overview of the experimental investigation of interest to the present work identified four fairly comprehensive studies of the deformation behavior of polyurea. A brief description of each of the four studies is presented in the remainder of this section.

In each case, information regarding: (a) the polyurea chemistry, stoichiometry, and synthesis; (b) the type of experimental technique employed; (c) the strain-rate range covered; (d) nominal test temperature(s) employed; (e) the maximum true strain attained; and (f) examples of the typical results obtained, are provided.

2.1 Amirkhizi et al. (Ref 22)

Polyurea chemistry, stoichiometry, and synthesis

- Lightly crosslinked polyurea synthesized from a multifunctional (functionality = 2.4) isocyanate [Isonate® 2143L (Ref 23)] and a high-molecular weight diamine [Versalink® P1000 (Ref 24)] in a 1.05:1.0 proportion.

Type of experimental technique employed

- Unconfined and confined Split Hopkinson Pressure Bar (SHPB), see Appendix.

Engineering strain-rate range

- 2000-4000 s^{-1}

Nominal test temperature(s)

- 273-333 K

Maximum true strain

- 0.8 (unconfined)
- 0.1 (confined)

Typical results obtained

- Examples of the typical results obtained are displayed in Fig. 3(a) and (b).

2.2 Yi et al. (Ref 25)

Polyurea chemistry, stoichiometry, and synthesis

- Lightly crosslinked polyurea synthesized from a multifunctional (functionality = 2.4) isocyanate [Isonate® 2143L (Ref 23)] and a high-molecular weight diamine [Versalink® P1000 (Ref 24)] in a 1.04:1.0 proportion.

Type of experimental technique employed.

- Constant engineering-strain rate or constant true-strain rate unconfined and confined low-rate uniaxial compression test.
- Unconfined high-strain rate SHPB technique
- Cycling unconfined low-rate compression tests

Engineering strain-rate range

- 0.001-1.0 s^{-1} (low-strain-rate range)
- 1400-10,400 s^{-1} (high-strain-rate range)

Nominal test temperature(s)

- 298 K

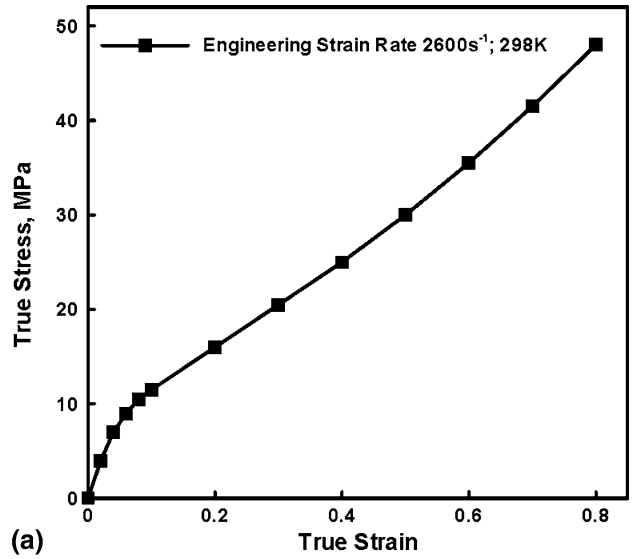

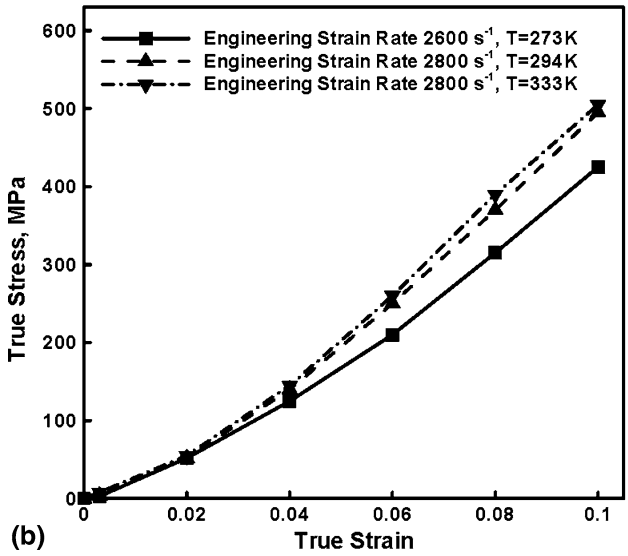

Fig. 3 Examples of the typical true-stress vs. true-strain experimental results obtained in Ref 22 for polyurea tested under; (a) unconfined; and (b) confined uniaxial compression loading conditions

Maximum true strain

- 1.0 (unconfined low-strain-rate compression)
- 0.12 (confined low-strain-rate compression)
- 1.5 (unconfined high-strain-rate compression)
- 1.0 (unconfined cyclic loading)

Typical results obtained

- Examples of the typical results obtained are displayed in Fig. 4(a)-(d).

2.3 Roland et al. (Ref 26)

Polyurea chemistry, stoichiometry, and synthesis

- Lightly crosslinked polyurea synthesized from a multifunctional (functionality = 2.4) modified isocyanate [Isonate® 2143L (Ref 23)] and a high-molecular weight diamine [Versalink® P1000 (Ref 24)] in a 1.04:1.0 proportion.

Type of experimental technique employed

- Drop-weight tensile test instrument

Engineering strain-rate range

- 0.15-573 s^{-1}

Nominal test temperature(s)

- 298 K

Maximum true strain

- 1.9

Typical results obtained

- Examples of the typical results obtained are displayed in Fig. 5.

2.4 Sarva et al. (Ref 27)

Polyurea chemistry, stoichiometry, and synthesis

- Same as in work of Yi et al. (Ref 25)

Type of experimental technique employed

- Low-moderate-strain-rate unconfined compression tests
- Moderate-intermediate-strain-rate unconfined compression tests
- High-strain-rate unconfined SHPB.

Engineering strain-rate range

- 0.0016-0.1 s^{-1} (low-moderate-strain-rate range)
- 1.0-100 s^{-1} (moderate-intermediate-strain-rate range)
- 100-1000 s^{-1} (intermediate-high-strain-rate range)
- >1000 s^{-1} (high-strain-rate range)

Nominal test temperature(s)

- 298 K

Maximum true strain

- 1.2

Typical results obtained

- Examples of the typical results obtained are displayed in Fig. 6.

3. Overview of the Prior Material Modeling Efforts

A review of the literature carried out as part of the present work revealed the existence of six material models specifically

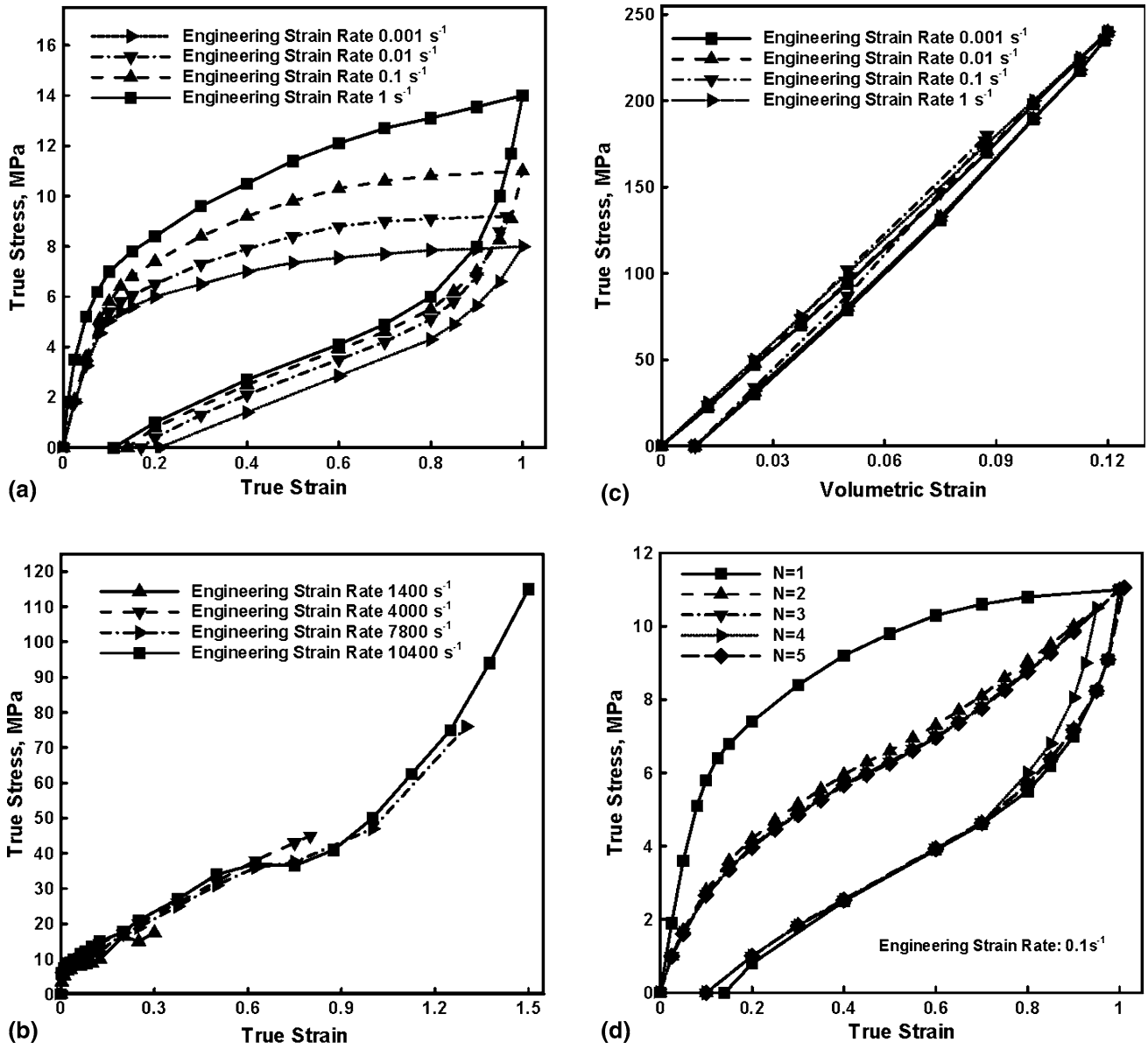

Fig. 4 Examples of the typical true-stress vs. true-strain experimental results obtained in Ref 25 for polyurea tested under; (a) unconfined; (b) and (c) confined; and (d) cyclic uniaxial compression loading conditions

developed for polyurea (Ref 22, 28-32). These models are critically evaluated below.

3.1 Qi and Boyce (Ref 28)

This model was originally developed and parameterized for polyurethane. However, due to considerable similarities in the microstructure (e.g., the presence of hard and soft domains) and the mechanical response (e.g., the presence of the so-called "stretch-induced" softening, i.e., a loss of material stiffness due to prior loading) between polyurethanes and polyurea, the model is applicable to the latter material as well. The model is based on the following physical grounds: (a) the co-existence of soft matrix and hard domains; (b) the ability of the soft matrix to undergo large reversible strains; (c) the ability of hard domains and hard-domain and soft-matrix interfaces to dissipate energy via rate-dependent inelastic-deformation processes; and (d) a deformation-induced increase in the amount of soft matrix (and the associated loss of material stiffness), due to disintegration of the hard domains.

The model assumes that the contribution of the soft matrix on one side and the contribution of the hard domains and hard-domain/soft-matrix interfaces on the other can be represented by two parallel branches, respectively. The first soft-matrix branch is modeled using the Arruda-Boyce HE formulation (Ref 33) in the form:

$$\sigma^{\mathrm{HE}} = \frac{v_s X \mu}{3J}\frac{\sqrt{N}}{\Lambda_{\mathrm{chain}}} L^{-1}\left(\frac{\Lambda_{\mathrm{chain}}}{\sqrt{N}}\right)\bar{B}', \qquad \text{(Eq 1)}$$

where v_s is effective volume fraction of soft matrix, $J = \det[F^{\mathrm{HE}}]$ (F^{HE} is the deformation gradient acting on the HE rubbery network and is equal to the total deformation gradient F), det denotes a determinant operator, $X = 1 + 3.5(1 - v_s) + 18(1 - v_s)^2$ is the soft-matrix strain-amplification factor, μ and N are Arruda-Boyce material constants, Λ_{chain} is

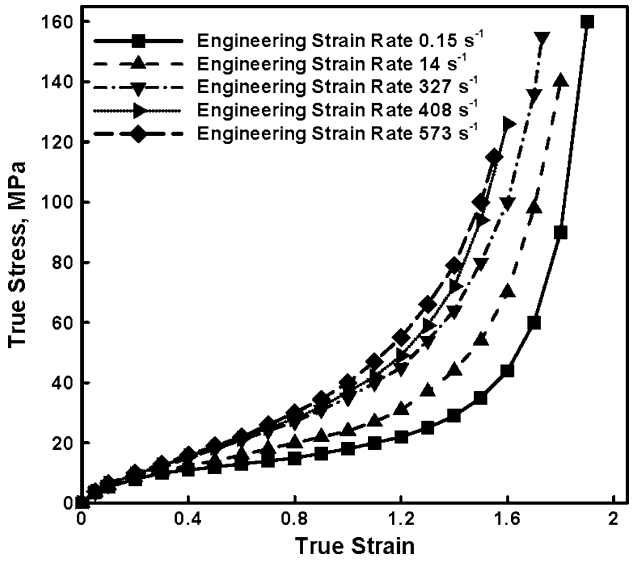

Fig. 5 Examples of the typical true-stress vs. true-strain experimental results obtained in Ref 26 for polyurea tested under uniaxial compression loading conditions

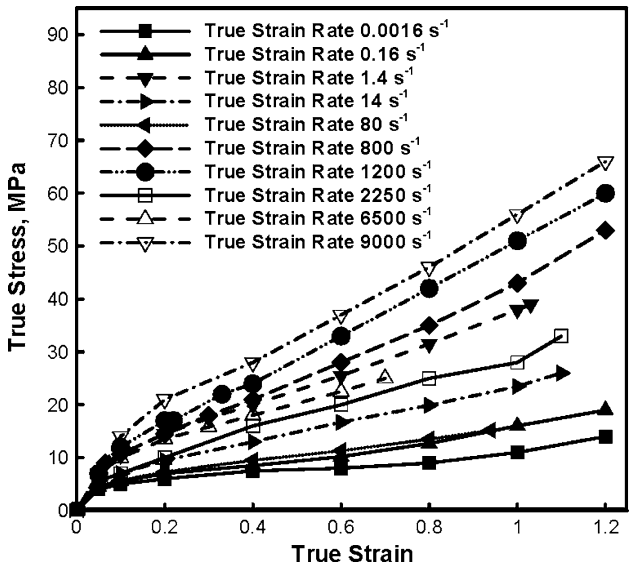

Fig. 6 Examples of the typical true-stress vs. true-strain experimental results obtained in Ref 27 for polyurea tested under unconfined uniaxial compression loading conditions

the "amplified" stretch in the eight-chain Arruda-Boyce model and is defined as $\Lambda_{chain} = \sqrt{X(\lambda_{chain}^2 - 1) + 1}$ (λ_{chain} is the corresponding chain stretch), L^{-1} is the inverse of Langevin function defined as $L(\beta) = \coth\beta - \frac{1}{\beta}$, $\bar{B} = \bar{F}^{HE}\bar{F}^{HE^T}$ is the isochoric left Cauchy-Green deformation tensor ($\bar{F}^{HE} = J^{-1/3}F^{HE}$) and is used to denote a deviator.

It should be noted that there are two modifications in Eq 1 relative to its standard form: (a) to account for the fact that in a unit volume of polyurea only v_s portion is filled with the soft matrix, a v_s multiplier is introduced and; (b) to account for the fact that the elastic deformation is mainly localized within the soft matrix, the average stretch within each of the Arruda-Boyce eight chains, λ_{chain}, is replaced with an amplified counterpart, Λ_{chain}. In addition, v_s is not considered as a constant but rather a quantity which increases with deformation. Hence, an evolution equation (given later in this section) is proposed for v_s in Ref 28.

The Cauchy stress within the second (elastic/visco-plastic, EVP) branch is next defined as:

$$\sigma^{EVP} = \frac{v_h}{J^E} L^E [\ln V^E], \qquad \text{(Eq 2)}$$

where $v_h = 1 - v_s$ is the hard-domain volume fraction, $J^E = \det(F^E)$ represents the Jacobian of the elastic part of $F^{EVP}(=F = F^{HE})$ resulting from multiplicative decomposition $F^{EVP} = F^E F^{VP}$, L^E is the fourth order elastic stiffness tensor, and $\ln V^E$ is the logarithmic strain, V^E is the left elastic stretch tensor resulting from the polar decomposition, $F^E = V^E R^E$ ($R^E = R$ is the rotation tensor). Equation 2 represents six equations with 12 (six σ^{EVP} components and six V^E components) unknowns.

It should be noted that while F^{EVP} maps the reference configuration into the current configuration, it is F^{VP} that maps the initial configurations into the so-called "relaxed configuration" (i.e., the configuration which is obtained by elastic unloading from the current configuration). Using the standard definition of the velocity gradient, L, the velocity gradient corresponding to F^{VP} is defined as $L^{VP} = \dot{F}^{VP}(F^{VP})^{-1} = D^{VP} + W^{VP}$, where D^{VP} and W^{VP} are the visco-plastic deformation rate and spin, respectively. Next without loss of generality, W^{VP} is set to zero and D^{VP} is set equal to L^{VP}. The flow rule is then defined as:

$$D^{VP} = \dot{F}^{VP}\left(F^{VP}\right)^{-1} = \dot{\gamma}^{VP}\frac{\bar{T}'}{\sqrt{2}\bar{\tau}}, \qquad \text{(Eq 3)}$$

where $\dot{\gamma}^{VP}$ is the equivalent visco-plastic shear strain rate, $\bar{T}'$ is (deviatoric) Cauchy stress mapped onto the relaxed configuration and $\bar{\tau} = \frac{1}{\sqrt{2}}|\bar{T}'|$ is the equivalent shear stress associated with the $\bar{T}'$ stress, $|\ldots|$ stands for the magnitude of a quantity.

The following constitutive definition of $\dot{\gamma}^{VP}$ was proposed:

$$\dot{\gamma}^{VP} = \dot{\gamma}_0 \exp\left[-\frac{\Delta G}{k\theta}\left\{1 - \frac{\bar{\tau}}{s}\right\}\right], \qquad \text{(Eq 4)}$$

where $\dot{\gamma}_0$ is the (thermal-activation based) preexponential (frequency) reference-rate term, ΔG is the zero- $\bar{\tau}$ activation energy, k is the Boltzmann's constant, θ is the temperature, and s the so-called "athermal" shear strength which represents the long-range resistance to visco-plastic deformation and is defined as:

$$s = \left(\frac{v_h}{v_{h_0}}\right)s_0, \qquad \text{(Eq 5)}$$

where v_{h_0} is the initial hard-domain volume fraction and s_0 is the initial value of s.

Equation 2, 3, and 4, represent a system of 13 equations with 13 unknowns (six σ^{EVP} components, six F^E components, and $\dot{\gamma}^{VP}$). However, before these equations can be solved, stress $\bar{T}$ (its deviator and invariants, like $\bar{\tau}$) have to be converted into their Cauchy stress counterparts. This is done through the use of the following relation:

$$\bar{T} = J^E\left(R^E\right)^T \sigma R^E, \qquad \text{(Eq 6)}$$

where $R^E = R$ due to the irrotational nature ($W^{VP} = 0$) of the visco-plastic part.

On obtaining the solution of the foregoing system of equations for σ^{EVP}, the contributions of the two branches σ^{HE} and σ^{EVP} are added to obtain the complete Cauchy stress.

To carry out this procedure for additional time steps, the soft-matrix volume fraction, v_s, must be updated. This is done using the following integrated form:

$$v_s = v_{ss} - (v_{ss} - v_{s_0}) \exp\left(-A \frac{\Lambda_{chain} - 1}{\lambda_{chain}^{lock} - \Lambda_{chain}}\right), \quad \text{(Eq 7)}$$

where v_{s_0} and v_{ss} are the initial and saturation values of v_s, λ_{chain}^{lock} is the locking stretch of the chain ($v_s \rightarrow v_{ss}$ as $\Lambda_{chain} \rightarrow \lambda_{chain}^{lock}$) and A is a parameter that characterizes the evolution in v_s with increasing Λ_{chain}.

There are two main concerns regarding this model: (a) all the rate dependence has been attached to the hard domains (and the hard-domain/soft-matrix interfaces), i.e., no account is given of the visco-elasticity in the soft matrix; and (b) the relations pertaining to the evolution of volume fraction of the soft matrix and of the athermal shear strength of the hard domains are defined using phenomenological approaches which do not account for the underlying microstructural processes in polyurea and the relations used are essentially borrowed from the related filled-rubber problems.

3.2 Amirkhizi et al. (Ref 22)

Within this model, the hydrostatic response of the material is considered to be isotropic temperature-dependent geometrically nonlinear/materially linear elastic while the deviatoric response of the material is assumed to be time-dependent and treated using a geometrically nonlinear/materially linear isotropic visco-elastic formulation.

Within the hydrostatic part of the model, pressure is defined as:

$$P = -K(\theta)\frac{\ln(J)}{J}; \quad K(\theta) = K(\theta_{ref}) + m(\theta - \theta_{ref}), \quad \text{(Eq 8)}$$

where subscript ref is used to denote a quantity at the reference temperature, K is the bulk modulus, and m is a material parameter.

To account for the aforementioned time-dependent character of the deviatoric material response, the deviatoric Cauchy stress, σ', is evaluated within the model by taking into consideration the entire deformation history of a given material point from the onset of loading at $t = 0$ to the current time, t, as:

$$\sigma'(t) = 2G_\infty \frac{\theta}{\theta_{ref}} \int_0^t \left(1 + \sum_{i=1}^{n} p_i \exp\left(\frac{-(\xi(t) - \xi(\tau))}{q_i}\right) D'(\tau)\right) d\tau, \quad \text{(Eq 9)}$$

where G_∞ is the "long-term" shear modulus (i.e., the value of the shear modulus after infinitely long-relaxation time), n is the number of terms in the Prony series exponential-type relaxation function, p_i and q_i are, respectively, the strength and the relaxation time of each Prony series term, ξ is the so-called reduced time, and D' ($=D - 1/3 * \text{tr}(D) * I$, tr denotes trace operator and I an identity tensor) is the deviatoric part of the rate of deformation tensor, D $(=\text{sym}(\dot{F}F^{-1})$,where "sym," the raised dot and superscript "−1", are used to denote, respectively, the symmetric part, the time derivative, and the inverse of a second-order tensor).

It is important to note that the Eq 9 is not objective and that its use is justified only under conditions of small rotation. For Eq 9 to become objective under large-rotation cases, it must be properly modified by replacing the deviatoric stress rate (in the integrand of Eq 9) by one of its objective counterparts. Since this modification is of a pure kinematic nature, it can be readily implemented but the resulting formulation is associated with a significantly higher computational cost.

To account for the effect of temperature and pressure on the kinetics of relaxation processes responsible for the observed visco-elastic behavior, the concept of reduced time is used as:

$$\xi(t) = \int_0^t \frac{dt}{10^{A(\theta - C_{TP}P - \theta_{ref})/(B + \theta - C_{TP}P - \theta_{ref})}}, \quad \text{(Eq 10)}$$

where A, B, and C_{TP} are material constants. Thus, the effect of temperature, θ, and pressure, P, over a time period t on the material response is assumed to be identical to the material response at the reference temperature and pressure over a time period $\xi(t)$. It should be noted that through the use of the reduced time concept, the effect of temperature is modeled by changing the time scale while leaving the material parameters p_i and q_i constant and equal to their values at the reference temperature.

To determine temporal evolution of the temperature, an adiabatic assumption is invoked, i.e., it is assumed that there is no heat transfer and that the rate of change of the local internal thermal energy is equal to the corresponding rate of dissipative work as:

$$C_v\dot{\theta} = \frac{\partial W_d}{\partial t} = 2G_\infty \frac{\theta(t)}{\theta_{ref}} \sum_{i=1}^{n} \frac{p_i}{q_i} \varepsilon_d^i(t) : \varepsilon_d^i(t), \quad \text{(Eq 11)}$$

where C_v is the constant volume specific heat, $\dot{\theta}$ is the temperature change rate, and ε_d is the dissipative strain defined as:

$$\varepsilon_d^i(t) = \int_0^t e^{-\frac{(\xi(t) - \xi(\tau))}{q_i}} D'(\tau) d\tau \quad \text{(Eq 12)}$$

At the first glance, evaluation of the stress appears straight forward through the use of Eq 8 and 9. However, this would require that Eq 9 be integrated from $t = 0$ at each time step (an extremely high-computational cost). To overcome this problem, concepts of the "creep" (i.e., elastic) and "dissipative" (i.e., viscos) strains within each branch are used so that $\sigma'(t + \Delta t)$ is computed as $\chi\sigma'(t) + \Delta\sigma'(t)$, where scaling χ accounts for stress relaxation of $\sigma'(t)$ during the $t + \Delta t$ time interval.

A summary of all the parameters for this polyurea material model is shown in Table 2 in Ref 22.

Critical assessment of this model identified three points of concern: (a) the aforementioned lack of objectivity under large rotations; (b) lack of inclusion of the so-called "stretch-induced" softening (i.e., a loss of material stiffness due to prior loading); and (c) the use of the reduced time concept is based on the so-called "time-temperature superposition" principle. Since different vibrational modes, e.g., segmental, chain, etc. are present within polyurea, for the reduced time approach to be valid all these modes must be equally affected by temperature (which is typically not the case).

3.3 Li and Lua (Ref 29)

Within this model, the hydrostatic response of the material is considered to be incompressible. Consequently the model, in its original formulation can only be used in the deformation analysis in which pressure can be assessed through alternative means. For example, in the uniaxial stress case, the zero stress condition in the lateral directions enables the determination of the pressure. As far as the deviatoric response is concerned, it is assumed to be the result of responses of two parallel branches, one HE and one viscoelastic (the viscoelastic branch is, in turn, allowed to contain multiple parallel viscoelastic subbranches). The HE branch which controls material mechanical response under low-deformation rates is represented using the Ogden-type model (Ref 30) and the corresponding strain energy density function is defined as:

$$W = \sum_{i=1}^{n} \frac{2\mu_i}{\alpha_i^2}\left(\lambda_1^{\alpha_i} + \lambda_2^{\alpha_i} + \lambda_3^{\alpha_i} - 3\right), \qquad \text{(Eq 13)}$$

where μ_i and α_i (i = 1, 2,…,n; n is the number of branches) are material-model parameters and λ_1, λ_2, and λ_3 (=$1/(\lambda_1\lambda_2)$) are the principal stretches. By using the standard relationships between: (a) the right Cauchy-Green deformation tensor, C, and the green strain E; (b) the Green-strain gradient of the strain energy and the second Piola Kirchoff stress; (c) the Cauchy stress and the second Piola Kirchoff stress and by recognizing that λ_1^2, λ_2^2, and λ_3^2 are eigen values of C, an expression for the Cauchy stress within the HE branch is derived (Eq 4) in Ref 29.

As far as the visco-elastic branch(s) is concerned, it was handled in a manner similar to Eq 9. The main difference is that the stress equation is made objective here by carrying out the required time integration within the reference configuration and then mapping the resulting second Piola Kirkhoff stress to the current configuration to obtain:

$$\sigma^{\mathrm{VE}} = -p^{\mathrm{VE}}I + F(v)\int_0^t \phi(I_1, I_2)m(t-\tau)\dot{E}(\tau)d\tau F^T(t), \qquad \text{(Eq 14)}$$

where $\phi(I_1, I_2)$ is the material-nonlinearity visco-elastic kernel, $m(t-\tau)$ is a relaxation function containing the contribution of all the viscoelastic branches and $\dot{E}$ is the (objective) Green-strain rate.

The total Cauchy stress is then obtained by summing the HE and visco-elastic contributions. The computational procedure employed to calculate σ^{VE} follows closely that used by Amirkhizi et al. (Ref 22). A summary of all the parameters for this polyurea material model is shown in Table 1 in Ref 29.

Critical assessment of this model identified that, with the exception of the problem related to the lack of objectivity, this model suffers from similar deficiencies as the one of Amirkhizi et al. (Ref 22).

3.4 Jiao et al. (Ref 31)

This model is quite similar to the Qi and Boyce model (Ref 28) and considers the presence of two branches, on HE and the other elastic/visco-plastic. However, in contrast to Qi and Boyce model (Ref 28): (a) the first branch is represented using the Neo-Hookean HE formulation; (b) no account is given to the fact that this branch is associated with the soft matrix (i.e., no v_s multiplier was used); (c) neither soft-matrix strain amplification nor evolution of the soft-matrix volume fraction is considered. Consequently, the Cauchy stress within the HE branch is defined as:

$$\sigma^{\mathrm{HE}} = \frac{2C_{10}}{J^{5/3}}(B') + K^{\mathrm{HE}}\ln[J]I, \qquad \text{(Eq 15)}$$

where $2{\cdot}C_{10}$ is the initial shear modulus, B' is the deviatoric part of the left Cauchy deformation tensor, $B(=FF^T)$ and K^{HE} is the bulk modulus.

In the second (visco-plastic) branch, the Cauchy stress is considered to be a sum of a deviatoric and a pressure term as:

$$\sigma^{\mathrm{VP}} = \sigma'^{\mathrm{VP}} - p^{\mathrm{VP}}I \qquad \text{(Eq 16)}$$

where σ'^{VP} is defined using the following linear relation:

$$\sigma'^{\mathrm{VP}} = 2\mu\ln V^{\mathrm{E}} - \frac{2\mu}{3}\mathrm{tr}\left(\ln V^{\mathrm{E}}\right)I, \qquad \text{(Eq 17)}$$

where μ is the second-branch shear modulus. In Eq 17, the only unknown is V^{E} which can be determined once $F^{\mathrm{E}}=F(F^{\mathrm{VP}})^{-1}$ is determined. Toward that end, the following flow rule is defined in the current configuration

$$D^{\mathrm{VP}} = \mathrm{sym}(L^{\mathrm{VP}}) = \mathrm{sym}\left(F^{\mathrm{E}}\dot{F}^{\mathrm{VP}}F^{\mathrm{VP},-1}F^{\mathrm{E},-1}\right) = \dot{\gamma}^{\mathrm{VP}}\frac{\sigma'^{\mathrm{VP}}}{|\sigma'^{\mathrm{VP}}|/\sqrt{2}} \qquad \text{(Eq 18)}$$

where it is, as in the Qi and Boyce model (Ref 28), again assumed that the visco-plastic spin $W^{\mathrm{VP}} = L^{\mathrm{VP}} - D^{\mathrm{VP}}$ is zero (i.e., plastic flow is irrotational, $L^{\mathrm{VP}} = D^{\mathrm{VP}}$). The visco-plastic equivalent shear strain rate $\dot{\gamma}^{\mathrm{VP}}$ is defined as

$$\dot{\gamma}^{\mathrm{VP}} = \dot{\gamma}_0 \exp\left(\frac{\tau_s - \tau_{s_0} - \alpha p}{\beta}\right), \qquad \text{(Eq 19)}$$

where $\dot{\gamma}_0$ is a material-dependent preexponential frequency term, $\tau_{s_0} = \Delta U/v$ (ΔU is the activation energy and v is the activation volume), $\alpha = \Omega(p)/v$ ($\Omega(p)$ is the pressure activation volume) and $\beta = k\theta/v$.

When Eq 17, 18, and 19 are combined one obtains 13 equations with 13 unknowns (six σ^{VP} components, six V^{E} components and $\dot{\gamma}^{\mathrm{VP}}$). The pressure within the visco-plastic branch is computed as a difference between the total pressure and the hyper-elastic pressure defined later. The total pressure is computed using the Lennard-Jones type relation as:

$$p = -A\left(J^{-N-1} - J^{-M-1}\right), \qquad \text{(Eq 20)}$$

where N = 6, M = 3 and A is one-sixth of the corresponding cohesive energy (defined by fitting the experimental data). Once the equations are solved, the σ^{VP} can be computed with σ^{HE} to obtain the total Cauchy stress.

This model suffers from the same deficiencies as the Qi and Boyce model (Ref 28). In addition, the model neglects the effect of hard-domain degradation and the associated loss of stiffness during deformation.

3.5 El Sayed (Ref 34)

This model considers the presence of one HE-plastic and several visco-HE branches, all connected in parallel. The HE response within each branch is modeled using an Ogden strain energy density function. The plastic (deviatoric + hydrostatic)

response of the first branch is considered to be strain and strain-rate hardenable while the visco-elastic response of the remaining branch(es) is treated using the Prony series formulism.

The HE strain energy density within all the HE branches is defined additively as:

$$W^{\mathrm{HE}} = W^{\mathrm{HE,vol}} + W^{\mathrm{HE,dev}}, \qquad \text{(Eq 21)}$$

where $W^{\mathrm{HE,vol}}$, the volumetric part of the strain energy function, is defined as:

$$W^{\mathrm{HE,vol}}(\varepsilon_{\mathrm{V}}^{\mathrm{HE}}, \theta) = \frac{K}{2}[\varepsilon_{\mathrm{V}}^{\mathrm{HE}} - h(\theta - \theta_0)]^2, \qquad \text{(Eq 22)}$$

where $\varepsilon_{\mathrm{V}}^{\mathrm{HE}}$ is the volumetric elastic logarithmic strain within a given branch and h is the thermal expansion coefficient, while, $W^{\mathrm{HE,dev}}$, the deviatoric part of the strain energy function, is represented using a Ogden-type model (Ref 30) as:

$$W^{\mathrm{HE,dev}}(e^{\mathrm{HE}}, \theta) = \sum_{j=1}^{3}\sum_{n=1}^{N}\frac{\mu_n}{\alpha_n}\left([\exp(e_j^{\mathrm{HE}})]^{\alpha_n} - 1\right), \qquad \text{(Eq 23)}$$

where N is the number of Ogden-terms considered (for time-invariant behavior), e_j^{HE} (j = 1,2,3) are the eigenvalues of e^{HE} (=dev($\varepsilon^{\mathrm{HE}}$), $\varepsilon^{\mathrm{HE}} = \frac{1}{2}\log(F^{\mathrm{HE}^T}F^{\mathrm{HE}})$.

3.5.1 HE/Plastic Branch. Within the first branch, the deformation gradient, F^{HE} can be calculated by multiplicative decomposition of F^{HEP} (=F=F^{HE} F^{P})) and $\varepsilon_{\mathrm{V}}^{\mathrm{HE}} = \mathrm{tr}(\varepsilon^{\mathrm{HE}})$. The strain energy functions given in Eq 22 and 23 are next differentiated with respect to $\varepsilon_{\mathrm{V}}^{\mathrm{HE}}$ and e_j^{HE}, respectively, to get the pressure and the principal deviatoric Cauchy stresses, p and σ_j^{HEP}, in the first (HE-plastic) branch as: $p^{\mathrm{HEP}} = -\frac{\partial W^{\mathrm{HE,vol}}}{\partial \varepsilon_{\mathrm{V}}^{\mathrm{HE}}}$ and $\sigma_j^{\mathrm{HEP}\prime} = \sum_{n=1}^{N}\mu_n \exp(e_j^{\mathrm{HE}})^{\alpha_n}$. The total Cauchy stress is then given by:

$$\sigma^{\mathrm{HEP}} = -p^{\mathrm{HEP}}I + \sum_{j=1}^{3}\sigma_j^{\mathrm{HEP}\prime} z_j \otimes z_j, \qquad \text{(Eq 24)}$$

where "$\otimes$" indicates a dyadic product and z_j are unit-norm deviatoric Cauchy-stress/strain eigen vectors.

It should be noted that in order to compute the Cauchy stress in the first branch via Eq 24, it is necessary to determine the elastic deformation gradient F^{HE}(=$F\cdot(F^{\mathrm{P}})^{-1}$)). This is done using the following flow rule:

$$\dot{F}^{\mathrm{P}}(F^{\mathrm{P}})^{-1} = \dot{\varepsilon}_{\mathrm{V}}^{\mathrm{P}}N^{\mathrm{P}} + \dot{\varepsilon}^{\mathrm{P}}M^{\mathrm{P}}, \qquad \text{(Eq 25)}$$

where N^{P} and M^{P} are plastic flow directions (second-order tensors subject to following normality constraints: tr(N^{P}) = $\pm$1; tr(M^{P}) = 0 and M^{P}:M^{P} = 3/2), $\dot{\varepsilon}_{\mathrm{V}}^{\mathrm{P}}$ is the effective volumetric plastic strain rate and $\dot{\varepsilon}^{\mathrm{P}}$ is the effective deviatoric plastic strain rate. The two plastic flow directions are, respectively, defined as:

$$M^{\mathrm{P}} = \sqrt{\frac{3}{2}}\frac{\sigma^{\mathrm{HEP}\prime}}{|\sigma^{\mathrm{HEP}\prime}|} \qquad \text{(Eq 26)}$$

and

$$N^{\mathrm{P}} = \frac{1}{3}\mathrm{sgn}(p^{\mathrm{HEP}})I \qquad \text{(Eq 27)}$$

where sgn(…) represents the sign operator.

Equation 25 introduced two new variables, $\dot{\varepsilon}_{\mathrm{V}}^{\mathrm{P}}$ and $\dot{\varepsilon}^{\mathrm{P}}$, which can be handled using the volumetric and the deviatoric yield criteria as:

$$\bar{p} - \bar{p}_{\mathrm{c}} = \frac{\partial \psi^{*,\mathrm{vol}}}{\partial \dot{\varepsilon}_{\mathrm{V}}^{\mathrm{P}}}, \qquad \text{(Eq 28)}$$

where $\bar{p} = \left(\frac{\partial W^{\mathrm{HE,vol}}}{\partial \varepsilon_{\mathrm{V}}^{\mathrm{HE}}}\right)$ is the effective pressure, $\bar{p}_{\mathrm{c}} = \left(\frac{\partial W^{\mathrm{P,vol}}}{\partial \varepsilon_{\mathrm{V}}^{\mathrm{P}}}\right)$; where $W^{\mathrm{P,vol}}(\varepsilon_{\mathrm{V}}^{\mathrm{P}}, \theta) = \frac{n\sigma_0(\theta)\varepsilon_0^{\mathrm{P}}}{n+1}N_{\mathrm{v}}\frac{4\pi a^3}{3}g(\varepsilon_{\mathrm{V}}^{\mathrm{P}}, n)$; $\sigma_0(\theta)$ is the initial yield strength; a is the void radius (volumetric plasticity is assumed to be associated with void dilation/contraction); n is the hardening exponent; N_{v} is the void density; f (=$(f_0 + J^{\mathrm{P}} - 1)/J^{\mathrm{P}}$; where f_0 is the initial void volume fraction given by $f_0 = N_v\frac{4\pi a_0^3}{3}$,, a_0 is the initial void radius; $g(\varepsilon_{\mathrm{V}}^{\mathrm{P}}, n) = \int_1^{1/f}\left(1 + \frac{2}{3\varepsilon_0^{\mathrm{P}}}\log\frac{x}{x-1+\frac{f_0}{f_0+\exp\varepsilon_{\mathrm{V}}^{\mathrm{P}}-1}}\right)^{\frac{n+1}{n}}dx$ and $\varepsilon_0^{\mathrm{P}}$ is the reference deviatoric plastic strain rate) is the volumetric yield strength and $\psi^{*,\mathrm{vol}}$ is the volumetric part of the kinetic potential given by:

$$\psi^{*,\mathrm{vol}}(J^{\mathrm{P}}, \dot{\varepsilon}_{\mathrm{V}}^{\mathrm{P}}, \theta) = \frac{m^{\mathrm{P}}\sigma_0(\theta)\dot{\varepsilon}_0^{\mathrm{P}}}{m^{\mathrm{P}}+1}N_{\mathrm{v}}\frac{4\pi a^3}{3}\left(1 - f^{\frac{1}{m^{\mathrm{P}}}}\right)\left|\frac{2\dot{a}}{\dot{\varepsilon}_0^{\mathrm{P}}a}\right|^{\frac{m^{\mathrm{P}}+1}{m^{\mathrm{P}}}} \qquad \text{(Eq 29)}$$

where m^{P} is the rate sensitivity exponent and $\dot{\varepsilon}_0^{\mathrm{P}}$is the reference plastic strain rate) is the void volume fraction. The deviatoric part of the yield criterion is given by:

$$\bar{\sigma} - \bar{\sigma}_{\mathrm{c}} = \frac{\partial \psi^{*,\mathrm{dev}}}{\partial \dot{\varepsilon}^{\mathrm{P}}}, \qquad \text{(Eq 30)}$$

where $\bar{\sigma} = \left(\frac{\partial W^{\mathrm{HE,dev}}}{\partial \bar{e}^{\mathrm{HE}}}, \bar{e}^{\mathrm{HE}} = \sqrt{\frac{2}{3}e^{\mathrm{HE}} : e^{\mathrm{HE}}}\right)$ is the effective deviatoric stress, $\bar{\sigma}_{\mathrm{c}}$ $\left(= \frac{\partial W^{\mathrm{P,dev}}}{\partial \varepsilon^{\mathrm{P}}}\right.$; ε^{P} is the effective deviatoric plastic strain; $W^{\mathrm{P,dev}}(\varepsilon^{\mathrm{P}}, \theta) = \left.\frac{n\sigma_0(\theta)\varepsilon_0^{\mathrm{P}}}{n+1}\left(1 + \frac{\varepsilon^{\mathrm{P}}}{\varepsilon_0^{\mathrm{P}}}\right)^{\frac{n+1}{n}}\right)$ is the deviatoric yield strength and $\psi^{*,\mathrm{dev}}$ is the deviatoric part of the kinetic potential given by:

$$\psi^{*,\mathrm{dev}}(\dot{\varepsilon}^{\mathrm{P}}, \theta) = \frac{m^{\mathrm{P}}\sigma_0(\theta)\dot{\varepsilon}_0^{\mathrm{P}}}{m^{\mathrm{P}}+1}\left(\frac{\dot{\varepsilon}^{\mathrm{P}}}{\dot{\varepsilon}_0^{\mathrm{P}}}\right)^{\frac{m^{\mathrm{P}}+1}{m^{\mathrm{P}}}} \qquad \text{(Eq 31)}$$

When Eq 24, 25, and 30 are combined one obtains 13 equations with 13 unknowns (six $\sigma^{\mathrm{HEP}\prime}$ components, six e^{HE} components and $\dot{\varepsilon}^{\mathrm{P}}$) which can be solved to obtain the deviatoric stress in the first branch. Next, Eq 24, 25, and 28 can be combined to give three equations with three unknowns (p^{HEP}, $\varepsilon_{\mathrm{V}}^{\mathrm{P}}$, and $\varepsilon_{\mathrm{V}}^{\mathrm{HE}}$) which can be solved to yield the pressure in the first branch. The total stress is then calculated using Eq 24.

3.5.2 Visco-HE Branch. The HE strain energy density within the visco-HE branches is defined additively as:

$$W_i^{\mathrm{HE}} = W_i^{\mathrm{HE,vol}} + W_i^{\mathrm{HE,dev}}, \qquad \text{(Eq 32)}$$

where $W_i^{\mathrm{HE,vol}}$, the volumetric part of the strain energy function for the visco-HE branches, is defined as:

$$W_i^{\mathrm{HE,vol}}\left(\varepsilon_{\mathrm{V},i}^{\mathrm{HE}}, \theta\right) = \frac{K_i}{2}\left(\varepsilon_{\mathrm{V},i}^{\mathrm{HE}}\right)^2, \qquad \text{(Eq 33)}$$

where $\varepsilon_{\mathrm{V},i}^{\mathrm{HE}}$ is the volumetric elastic logarithmic strain in the ith visco-HE branch while, $W_i^{\mathrm{HE,dev}}$, the deviatoric part of the

strain energy function, is represented using a Ogden-type model as:

$$W_i^{\mathrm{HE,dev}}\left(e_i^{\mathrm{HE}},\theta\right)=\sum_{j=1}^{3}\sum_{n=1}^{N_i}\frac{\mu_{i,n}}{\alpha_{i,n}}\left(\left[\exp\left(e_{i,j}^{\mathrm{HE}}\right)\right]^{\alpha_{i,n}}-1\right), \quad \text{(Eq 34)}$$

where N_i is the number of Ogden-terms considered for time-infinity behavior in the ith visco-HE branch, $e_{i,j}^{\mathrm{HE}}$ $(j = 1,2,3)$ are the eigenvalues of e_i^{HE} $(=\mathrm{dev}(\varepsilon_i^{\mathrm{HE}})$, $\varepsilon_i^{\mathrm{HE}}=\frac{1}{2}\log(F_i^{\mathrm{HE}^T}F_i^{\mathrm{HE}})$ where F_i^{HE} can be calculated by multiplicative decomposition of F_i^{VHE} $(=F=F_i^{\mathrm{HE}}F_i^{\mathrm{V}})$ and $\varepsilon_{i,\mathrm{V}}^{\mathrm{HE}}=\mathrm{tr}(\varepsilon_i^{\mathrm{HE}})$. The viscous principal stresses are then calculated as:

$$\sigma_{i,j}^{\mathrm{VHE}}=\frac{\partial W_i^{\mathrm{HE}}}{\partial\varepsilon_{i,j}^{\mathrm{HE}}}, \quad \text{(Eq 35)}$$

where $\varepsilon_{i,j}^{\mathrm{HE}}$ are the eigen values of $\varepsilon_i^{\mathrm{HE}}$. The pressure in each visco-HE branch is then defined by the following expression:

$$p_i^{\mathrm{VHE}}=\frac{1}{3}\left(\sigma_{i,1}^{\mathrm{VHE}}+\sigma_{i,2}^{\mathrm{VHE}}+\sigma_{i,3}^{\mathrm{VHE}}\right) \quad \text{(Eq 36)}$$

The deviatoric principal stresses in each visco-HE branch are then calculated as:

$$\sigma_{i,j}^{\mathrm{VHE}\prime}=\sigma_{i,j}^{\mathrm{VHE}}-p_i^{\mathrm{VHE}} \quad \text{(Eq 37)}$$

Finally, the total Cauchy stress in each visco-HE branch is calculated as:

$$\sigma_i^{\mathrm{VHE}}=-p_i^{\mathrm{VHE}}I+\sum_{j=1}^{3}\sigma_{i,j}^{\mathrm{VHE}\prime}M_{i,j}^{\mathrm{V}}\otimes M_{i,j}^{\mathrm{V}}, \quad \text{(Eq 38)}$$

where $M_{i,j}^{\mathrm{V}}$ are unit-norm Cauchy-stress/deformation rate $\left(D_i^{\mathrm{V}}=\dot{F}_i^{\mathrm{V}}\left(F_i^{\mathrm{V}}\right)^{-1}\right)$ eigen vectors.

However, before the Cauchy stress in the ith visco-HE branch is computed, it is necessary to determine the elastic deformation gradient F_i^{HE} $(=F\cdot(F_i^{\mathrm{V}})^{-1})$. This is done using the following flow rule:

$$\dot{F}_i^{\mathrm{V}}\left(F_i^{\mathrm{V}}\right)^{-1}=\sum_{j=1}^{3}\dot{\varepsilon}_{i,j}^{\mathrm{V}}M_{i,j}^{\mathrm{V}}\otimes M_{i,j}^{\mathrm{V}}, \quad \text{(Eq 39)}$$

where $\dot{\varepsilon}_{i,j}^{\mathrm{V}}$ are the eigenvalues of $D_i^{\mathrm{V}}=\dot{F}_i^{\mathrm{V}}\left(F_i^{\mathrm{V}}\right)^{-1}$ (viscous spin is assumed to be zero). In order to compute the total Cauchy stress, an additional equation is necessary. This equation is the one for the viscous principal stresses:

$$\sigma_{i,j}^{\mathrm{VHE}}=\frac{\partial W_i^{\mathrm{HE,dev}}}{\partial e_{i,j}^{\mathrm{HE}}}=\frac{\partial\phi_i^{*,\mathrm{dev}}}{\partial\dot{e}_{i,j}^{\mathrm{V}}} \quad \text{(Eq 40)}$$

where

$$\phi_i^{*,\mathrm{dev}}\left(\dot{e}_i^{\mathrm{V}},\theta\right)=\sum_{j=1}^{3}\sum_{n=1}^{N_i}\frac{\eta_{i,n}^{\mathrm{dev}}}{\alpha_{i,n}}\left(\left[\exp\left(\frac{\dot{e}_{i,j}^{\mathrm{V}}}{\dot{e}_{0i,j}^{\mathrm{V}}}\right)\right]^{\alpha_{i,n}}-1\right), \quad \text{(Eq 41)}$$

where η^{dev} is a deviatoric viscous coefficient and, $\dot{e}_{i,j}^{\mathrm{V}}$ and $\dot{e}_{0i,j}^{\mathrm{V}}$ are the current and reference eigenvalues of the viscous strain rate.

When Eq 38, 39, and 40 are combined one obtains 12 equations with 12 unknowns (six σ_i^{VHE} components, three $e_{i,j}^{\mathrm{HE}}$ components and three $\dot{\varepsilon}_{i,j}^{\mathrm{V}}$ components) for each of the visco-HE branches which can be solved to obtain the Cauchy stress in each branch.

The model also takes into account the plastic expansion or contraction of voids and therefore the stresses are appropriately modified to account for the effect of microinertia (Ref 35, 36). However, for brevity, this portion of the model is not reviewed here.

The following main concerns have been identified with regard to this model:

(a) a relatively large number of parameters and a need for extensive parameter identification efforts; (b) the model is of a generic type and does not include any unique features associated with polyurea microstructure/response; and (c) the model was never validated under more general three-dimensional dynamic-loading conditions.

3.6 Grujicic et al. (Ref 32)

The two main differences between this model and the models described above are: (a) this model is of an equilibrium (time-invariant/quasi-static) type; and (b) a substantially larger degree of material's physics is used during the process of material-model formulation. That is, the key components of this material (mechanical) model are developed by first constructing a simple molecular-level microstructure model and by relating the microstructural elements and intrinsic material processes to the material mechanical response. For example, the evolution equation for the deformation-induced softening and inelasticity observed in polyureas is directly linked to the associated evolution of the soft-matrix/hard-segment molecular-level microstructure of this material.

Overall, the model can be characterized as being isotropic, hyper-elastic (with degradable elastic stiffness components) and rate-independent plastic. Consequently, at small strains, the mechanical response of polyurea is completely reversible, i.e., no permanent changes in the material microstructure or residual strains are observed. At larger strains, however, degradation/breakage of the hydrogen bonds within the hard segments of polyurea gives rise both to inelastic-deformation and stiffness-degradation effects. The model was fully parameterized using one set of open literature experimental data, validated against another set of experimental data and formulated as a general finite-strain HE/plastic three-dimensional material model and implemented into a user-material subroutine for easy incorporation into the commercial finite element programs. Additional details regarding this model can be found in Ref 32.

The main concern regarding this model is that it is of a quasi-static nature and, hence, of little utility with respect to its use in computer-aided engineering analyses of various shock/ballistic-impact scenarios.

4. Polyurea-slug impact on a rigid, fixed flat target

In this section, an attempt is made to compare the predictions of the six material models for polyurea overviewed in the previous section. Since the main application of polyurea considered here involves high-rate (shock-type) dynamic loading, the models are used within a simple transient nonlinear dynamics analysis to predict the three basic shock-Hugoniot relations: (a) axial-stress (σ_{11}) versus specific volume (v); (b) shock speed (U_s) versus particle velocity (u_p); and (c) mass-based internal energy density (e) versus v.

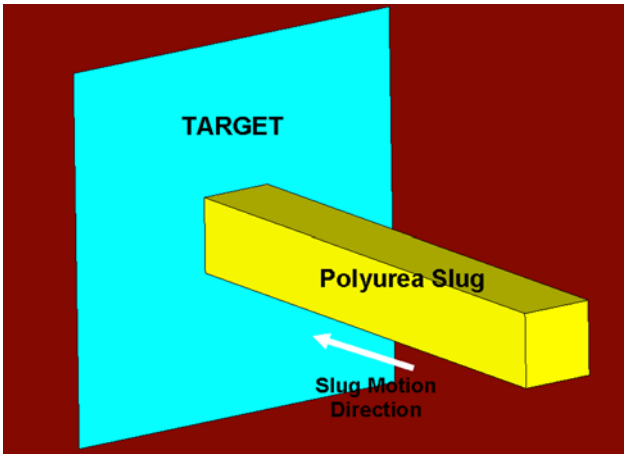

Fig. 7 A schematic of the zero-obliquity slug-impact problem involving a flat, rigid, fixed target

The computational analysis employed here considered the case of a rectangular slug hitting a rigid fixed flat target at a zero-obliquity angle. To mimic the more common conditions encountered near the center of the target surface associated with collision of a plate-like polyurea structure, zero normal lateral-strain and zero all-shear strain conditions are applied to the polyurea slug. Thus, the problem analyzed is essentially of a one-dimensional nature, Fig. 7.

The expected (and obtained) temporal evolution of the material within the slug following the impact can be described as follows: After impact, polyurea at the impacted end of the slug becomes compressed and a compressive shock wave begins to travel in the direction opposite to the slug-motion direction. Polyurea material particles swept by the compressive shock are brought to the state of rest. When the (densifying) shock wave reaches the free end of the slug, it reflects as a tensile wave (or more precisely as a release wave). The tensile wave then travels toward the target surface and all the polyurea material particles swept by this wave are imparted a velocity (i.e., a linear momentum) in the direction opposite to the initial motion-direction of the slug. When the release wave has managed to fully traverse the slug, all the particles are imparted this momentum and the slug, as a whole, separates from the target and continues to move in the direction opposite to the initial impact direction. It is this (residual) momentum of the slug that governs the extent of momentum transfer to the target surface.

4.1 Problem Formulation

As mentioned above, the basic problem analyzed in this section is the one-dimensional impact of a polyurea slug against a rigid, fixed flat target surface. The case of a 0.03-m long rectangular polyurea slug was considered in the present work (slug lateral dimensions are irrelevant due to the one-dimensional nature of the problem at hand). The initial volumetric state of polyurea is defined by its initial density ρ_{init} (=1100 kg/m^3).

4.2 Computational Procedure

The physical problem at hand is cast as a finite element problem and solved within a Lagrangian framework using ABAQUS/Explicit (Ref 37). Typically, 1000 eight-node first-order reduced-integration brick-type elements are used. The lateral nodal degrees of freedom are suppressed while all the slug nodes are initially assigned a constant velocity. The target is modeled as a rigid, fixed, flat analytical surface. Slug/target contact is modeled using a penalty contact algorithm. Within the penalty contact method, the penetration of the surfaces into each other is resisted by linear spring forces/contact pressures with values proportional to the depth of penetration. These forces, hence, tend to pull the surfaces into an equilibrium position with no penetration. Contact pressures between two bodies are not transmitted unless the nodes on the "slave surface" contact the "master surface." There is no limit to the magnitude of the contact pressure that could be transmitted when the surfaces are in contact. Transmission of shear stresses across the contact interfaces is defined in terms of a static and a kinetic/sliding friction coefficient and an upper-bound shear stress limit (a maximum value of shear stress which can be transmitted before the contacting surfaces begin to slide).

To accurately capture the shock/release wave-front structure, no artificial damping (a procedure which improves computational robustness) was used. Instead, the wave front was naturally stabilized by the accompanying energy dissipation processes.

Each of the polyurea models reviewed in the previous section is implemented as a VUMAT User-material subroutine and linked with the ABAQUS/Explicit (Ref 37) solver.

4.3 Results and Discussion

Examples of the typical results obtained in this portion of the work are displayed in Fig. 8(a)-(c).

Temporal evolution of the contact pressure at the slug/target interface at two levels of slug initial velocity (500 and 1000 m/s) is depicted in Fig. 8(a). Examination of the results displayed in Fig. 8(a) reveals that the magnitude of the contact pressure increases while slug-target contact time decreases with an increase in the slug initial velocity. It should be noted that the area under the contact pressure versus postimpact time curve is equal to the specific momentum transferred to the target during impact.

Spatial variation of the polyurea material-particle velocities (normalized by the slug initial velocity) at different postimpact times for the case of slug initial velocity of 1000 m/s is depicted in Fig. 8(b). It should be noted that (slug initial-length normalized) undeformed spatial coordinates are used as the abscissa in Fig. 8(b). Examination of the results displayed in Fig. 8(b) reveals that, as expected, impact of the slug against the rigid fixed target causes generation of a shock wave moving toward the free end of the slug (located at $x/L = 0.0$). The material swept by the shock wave has been brought into the zero velocity state. On the reflection of the shock wave from the slug free end, a release/tensile wave is generated and begins to move toward the target. In the slug region swept by the release wave, material particles are imparted a velocity opposite to the slug initial direction of motion.

Spatial variation of the polyurea density at different postimpact times for the case of slug initial velocity of 1000 m/s is depicted in Fig. 8(c). Examination of the results displayed in Fig. 8(c) reveals that these results are the expected counterparts of the results displayed in Fig. 8(b). Namely, shock loading of the slug densifies the material within the slug, while the passage of a subsequent release wave (not shown for brevity) reduces the density. These findings are in agreement

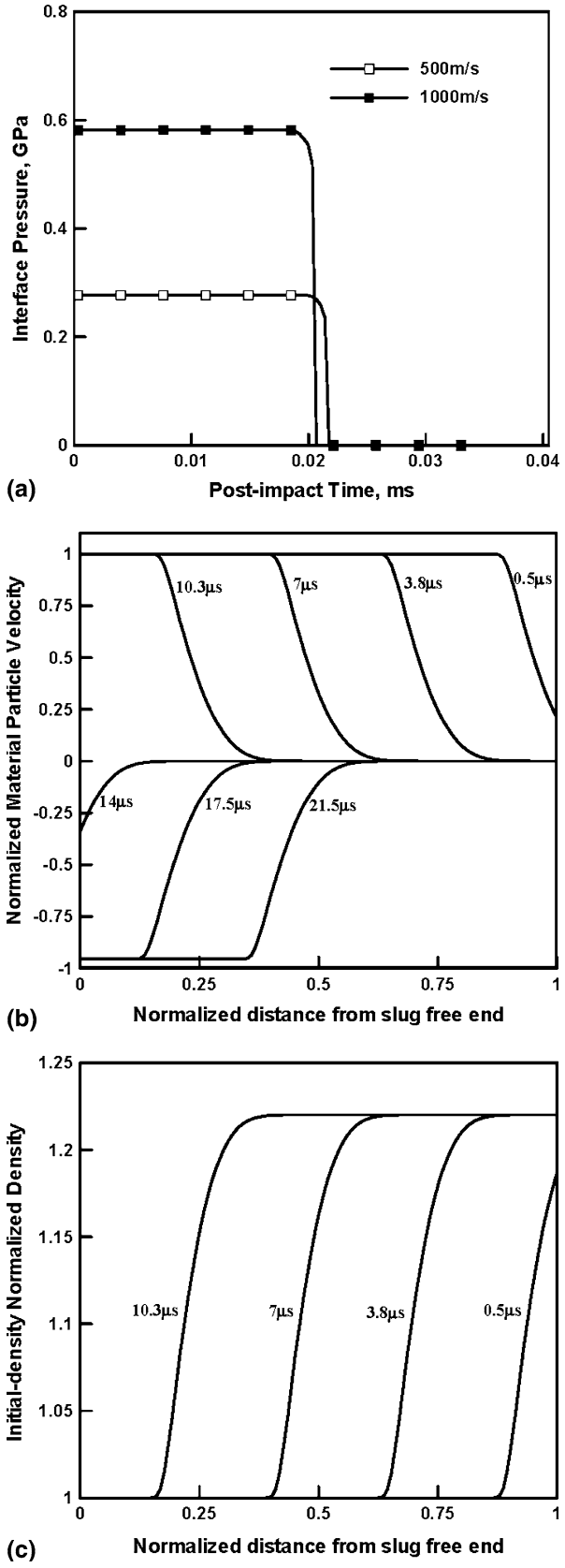

Fig. 8 (a) Temporal evolution of the slug/target contact pressure at two slug velocities (500 and 1000 m/s); and spatial distribution of (b) the (slug initial velocity) normalized polyurea density at different slug/target postimpact times for the case of 1000 m/s slug initial velocity

with the basic theory of shock-wave generation and propagation which states that at the shock front the material changes between the preshock and the postshock states along the so-called Rayleigh line (a line along which material state variables, such as the particle velocity and the mass density, are related via a simple functional relation).

To test the predictions of the six polyurea material models in the dynamic-loading regime, the results like the ones displayed in Fig. 8(a)-(c) are used to generate the three shock-Hugoniot relations mentioned earlier. A shock Hugoniot is a locus of material states attainable (for a given material initial state) after passage of shocks of various strengths. While the shock Hugoniot is defined within a multidimensional (stress-specific volume, specific energy density, particle velocity, temperature, shock velocity, …) space, it is generally displayed using the appropriate two-dimensional projections (e.g., σ_{11} versus v, U_s versus u_p, and ε versus v). It should be noted that the material model defines a surface in the same multidimensional (material state) space and that the Hugoniot is an intersection between this surface and a surface defining interrelationships between the same state variables behind the shock front in any material. Hugoniots are typically used to analyze the propagation and interaction of planar shock waves.

The six computed σ_{11} versus v shock Hugoniots obtained are displayed in Fig. 9(a). The σ_{11} data (at a given slug-impact velocity) were taken directly from the contact pressure versus time results (like the ones displayed in Fig. 8(a)). The corresponding specific-volume data are obtained by taking the reciprocal of the shocked-material densities (like the ones displayed in Fig. 8(c)). For comparison, the experimental data reported in Ref 38 are also shown in Fig. 9(a). Examination of the results displayed in Fig. 9(a) reveals that:

(a) the six polyurea models give rise to a vastly different axial stress versus specific volume Hugoniots;
(b) the overall best agreement between the computational and the experimental results is obtained in the case of the model of Grujicic et al. (Ref 32) with the model of Jiao et al. (Ref 31) being the second best;
(c) the observed poor prediction of the Qi and Boyce model (Ref 28) can be attributed to the fact that its parameterization was carried out by simply correlating the material parameters for polyurea to the Qi and Boyce material parameters for polyurethane; and
(d) the poor prediction of the model by Li and Lua (Ref 29) is the result of the fact that the model parameterization was carried out using uniaxial tensile experimental results and this parameterization is inherently incompatible with the compressive behavior of polyurea.

The six computed U_s versus u_p shock Hugoniots obtained are displayed in Fig. 9(b). The U_s data (at a given slug-impact velocity) is obtained by monitoring the shock-front position as a function of time (using the results like the ones displayed in Fig. 8(b), (c)). The particle velocity u_p is set equal to the slug initial velocity. For comparison, the experimental data reported in Ref 38 are also shown in Fig. 9(b). Examination of the results displayed in Fig. 9(b) reveals that the model of Jiao et al. (Ref 31) yields an excellent agreement with the experimental results. The remaining findings are consistent with the ones reported above in conjunction with Fig. 9(a).

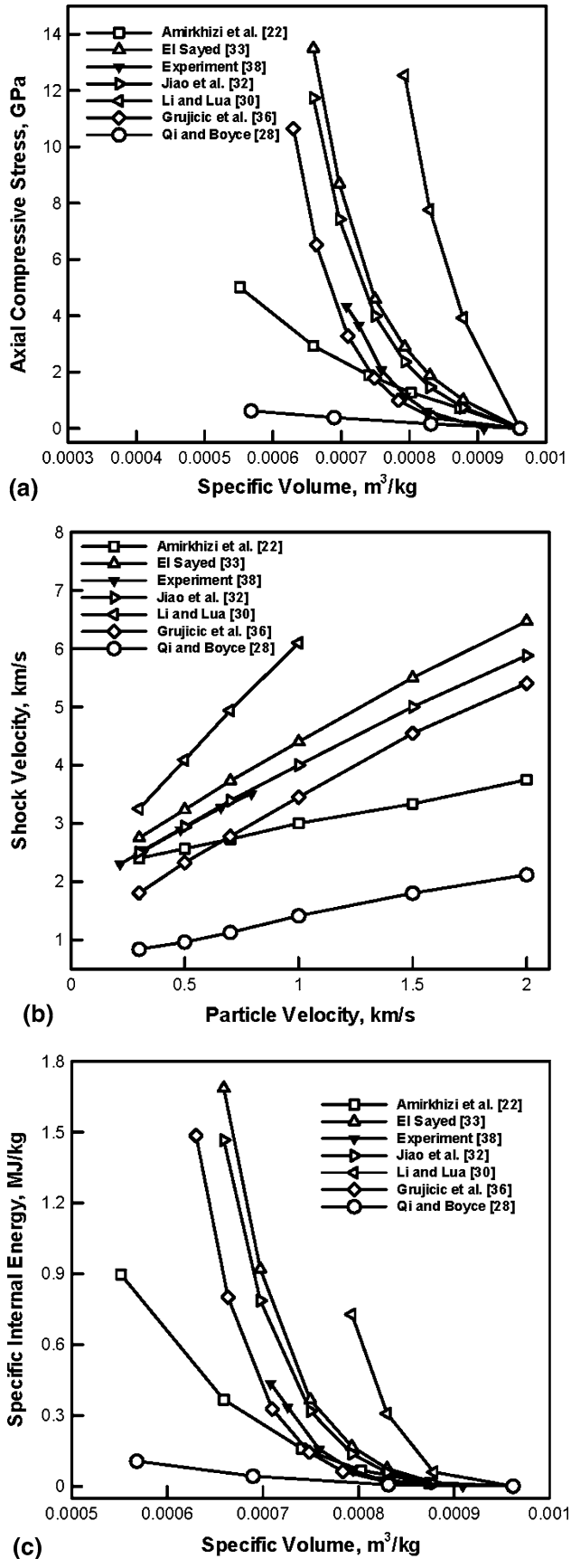

Fig. 9 A comparison between six computed shock Hugoniots and their experimental counterpart. The following shock Hugoniots are compared: (a) σ_{11} vs. v; (b) U_s vs u_p; (c) ε vs. v

The six computed ε versus v shock Hugoniots obtained are displayed in Fig. 9(c). The ε data (at a given slug-impact velocity) are obtained by combining the results displayed in Fig. 9(a) with the Rankine-Hugoniot equation (Ref 39). For comparison, the experimental data reported in Ref 38 is also shown in Fig. 9(c). Examination of the results displayed in Fig. 9(c) reveals that the extents of agreement between the various computed ε versus v Hugoniots and their experimental counterpart are comparable to those previously observed in the case of axial stress versus specific-volume Hugoniots, Fig. 9(a).

5. Summary and Conclusions

Based on the results obtained in the present work, the following main summary remarks and conclusions can be drawn:

1. A comprehensive overview of the main experimental efforts reported in the open literature pertaining to the characterization of the mechanical response of polyurea under various quasi-static and dynamic deformation modes is carried out.
2. A parallel comprehensive overview and a critical assessment of the material mechanical models for polyurea reported in the open literature are presented.
3. To test the validity/fidelity of the available polyurea material mechanical models, a transient nonlinear dynamics analysis of a polyurea slug impacting a flat, rigid, fixed target is carried out. The results obtained are used to construct the appropriate shock-Hugoniot relations which are in turn, compared with their experimental counterparts.
4. The aforementioned comparison established that, while different material models yield vastly different shock-Hugoniot relations, the predictions of a couple of the models are in reasonably good agreement with their experimental counterpart.

Acknowledgments

The material presented in this article is based on work supported by the Office of Naval Research (ONR) research contract entitled "Elastomeric Polymer-By-Design to Protect the Warfighter Against Traumatic Brain Injury by Diverting the Blast Induced Shock Waves from the Head," Contract Number 4036-CU-ONR-1125 as funded through the Pennsylvania State University. The authors are indebted to Dr. Roshdy Barsoum of ONR for continuing support and interest in the present work.

Appendix: Split Hopkinson Pressure Bar

The SHPB setup is used for determination of the high-strain-rate (unconfined or confined) compression stress versus strain data. As schematically represented in Fig. A1, an SHPB setup consists of a striker bar, an incident bar, the specimen being tested and the transmitter bar. A rectangular compression wave of well-defined amplitude and duration is generated in the incident bar when the incident bar is struck by the striker bar. When the wave reaches the incident bar/specimen interface, it is partially transmitted into the specimen (and subsequently)

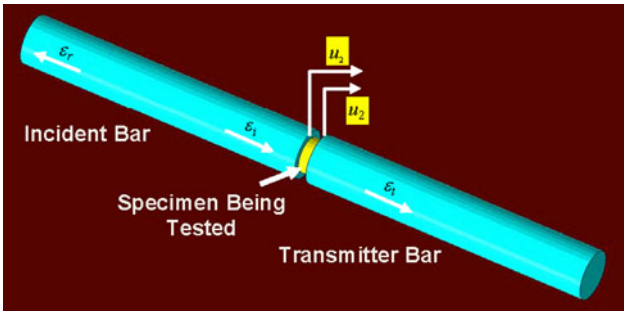

Fig. A1 A schematic of a Split Hopkinson Pressure Bar (SHPB) setup

into the transmitter bar, and partially reflected back to the incident bar.

Using a one-dimensional wave propagation analysis, it is possible, as shown below, to determine high-strain rate stress-strain curves from measurements of the temporal evolution of strain in the incident and transmitter bars.

Propagation of waves along the length of the bar (x direction) is, to a good approximation, governed by the one-dimensional wave equation:

$$\frac{\partial^2 u}{\partial x^2} - \frac{1}{c^2}\frac{\partial^2 u}{\partial t^2} = 0 \qquad \text{(Eq A.1)}$$

which has the solution within the incident bar:

$$u = f(x - ct) + g(x + ct) = f(z_1) + g(z_2) = u_\mathrm{i} + u_\mathrm{r}, \qquad \text{(Eq A.2)}$$

where u_i is the incident wave, u_r is the reflected wave, c is the speed of propagation of the wave, t time and z_1 and z_2 are single variables that f and g depend on, respectively. The corresponding axial strain in the incident bar is then defined as:

$$\varepsilon = \frac{\partial u}{\partial x} = \frac{\partial (u_\mathrm{i} + u_\mathrm{r})}{\partial x} \qquad \text{(Eq A.3)}$$

Substituting Eq A.3 into Eq A.2 yields:

$$\varepsilon = \frac{df}{dz_1}\frac{\partial z_1}{\partial x} + \frac{dg}{dz_2}\frac{\partial z_2}{\partial x} = \frac{df}{dz_1} + \frac{dg}{dz_2} = f' + g' = \varepsilon_\mathrm{i} + \varepsilon_\mathrm{r} \qquad \text{(Eq A.4)}$$

The velocity of any material point in the incident bar can be determined by differentiating Eq A.2 with respect to time as:

$$\dot{u} = \frac{\partial (u_\mathrm{i} + u_\mathrm{r})}{\partial t} = \frac{df}{dz_1}\frac{\partial z_1}{\partial t} + \frac{dg}{dz_2}\frac{\partial z_2}{\partial t} = -cf' + cg' = c(-f' + g') = c(-\varepsilon_\mathrm{i} + \varepsilon_\mathrm{r}) \qquad \text{(Eq A.5)}$$

In the case of the transmitter bar, there is only one wave, the transmitted wave, propagating through it (until the wave reflects at the free end of the transmitter bar, which takes place at a post data-collection time). Therefore, the velocity of the material points within the transmitter bar is obtained by differentiating, with respect to time, displacement field $u(t) = h(z_1) = h(x - ct)$ as:

$$\dot{u} = \frac{dh}{dz_1}\frac{\partial z_1}{\partial t} = -ch' = -c\varepsilon_\mathrm{t} \qquad \text{(Eq A.6)}$$

The strain rate in the specimen is next calculated as:

$$\dot{\varepsilon} = \frac{(\dot{u}_\mathrm{I/S} - \dot{u}_\mathrm{S/T})}{l_\mathrm{S}}, \qquad \text{(Eq A.7)}$$

where l_s is the instantaneous length of the specimen and subscripts I/S and S/T are used to, respectively, denote the velocities of the incident bar/specimen, Eq A.5 and the specimen/transmitter bar, Eq A.6, interfaces. Combining Eq A.5, A.6, and A.7, the instantaneous (average) strain rate in the specimen can be calculated from the measured time-dependent strains in the incident and the transmitter bars as:

$$\dot{\varepsilon} = \frac{c}{l_\mathrm{s}}(-\varepsilon_\mathrm{i} + \varepsilon_\mathrm{r} + \varepsilon_\mathrm{t}) \qquad \text{(Eq A.8)}$$

The corresponding strain in the specimen can be obtained by integrating over time the specimen strain rate.

To determine the axial stress in the specimen, the forces in the incident and transmitter bars are first determined. Since the two bars are deformed elastically, the corresponding forces are defined as:

$$F_\mathrm{I} = A_\mathrm{I}E_\mathrm{I}(\varepsilon_\mathrm{i} + \varepsilon_\mathrm{r}) \qquad \text{(Eq A.9)}$$

$$F_\mathrm{T} = A_\mathrm{T}E_\mathrm{T}\varepsilon_\mathrm{t} \qquad \text{(Eq A.10)}$$

where A and E are, respectively, used to denote the cross-sectional area and the Young's modulus of the incident (I) and the transmitter (T) bars.

The SHPB analysis presented here is based on the following two assumptions:

(a) after some initial ringing, the specimen is deformed uniformly. This assumption was already used in the case of Eq A.7; and
(b) the specimen is in the state of dynamic equilibrium, i.e., the forces acting at the I/S and the S/T interfaces are equal.

Under the conditions $A_\mathrm{I} = A_T$ and $E_\mathrm{I} = E_\mathrm{T}$, this assumption via Eq A.9 and A.10 yields:

$$\varepsilon_\mathrm{t} = \varepsilon_\mathrm{r} + \varepsilon_\mathrm{i} \qquad \text{(Eq A.11)}$$

Substituting Eq A.11 into Eq A.8 yields:

$$\dot{\varepsilon} = \frac{2c\varepsilon_\mathrm{r}}{l_\mathrm{s}} \qquad \text{(Eq A.12)}$$

suggesting that the specimen strain rate can be determined solely from the measured strains associated with the reflected wave within the incident bar.

The corresponding stress in the specimen is then calculated by dividing the force in the sample by the sample cross-sectional area as:

$$\sigma(t) = \frac{A_\mathrm{T}E_\mathrm{T}\varepsilon_\mathrm{t}}{A_\mathrm{s}} \qquad \text{(Eq A.13)}$$

Equation A.13 was obtained using Eq A.10. The same could be done using Eq A.11 or a mean of the Eq A.11 and A.12.

References

1. A.J. Ryan, Spinodal Decomposition During Bulk Copolymerization: Reaction Injection Molding, *Polymer*, 1989, **31**, p 707–712

2. C.M. Roland and R. Cassini, Effect of Hydrostatic Pressure on the Visco-elastic Response of Polyurea, *Polymer*, 2007, **48**, p 5747–5752
3. Y.A. Bahei-El-Din, G.J. Dvorak, and O.J. Fredricksen, A Blast-Tolerant Sandwich Plate Design With a Polyurea Interlayer, *Int. J. Solids Struct.*, 2006, **43**, p 7644–7655
4. R.B. Bogoslovov, C.M. Roland, and R.M. Gamache, Impact-Induced Glass-Transition in Elastomer Coatings, *Appl. Phys. Lett.*, 2007, **90**, p 221910
5. M. Grujicic, B. Pandurangan, and B.A. Cheeseman, A Computational Analysis of Detonation of Buried Mines, *Multidiscip. Model. Mater. Struct.*, 2006, **2**, p 363–387
6. M. Grujicic, B. Pandurangan, and B.A. Cheeseman, The Effect of Degree of Saturation of Sand on Detonation Phenomena Associated with Shallow-Buried and Ground-Laid Mines, *Shock Vib.*, 2006, **13**, p 41–62
7. M. Grujicic, B. Pandurangan, Y. Huang, B.A. Cheeseman, W.N. Roy, and R.R. Skaggs, Impulse Loading Resulting from Shallow Buried Explosives in Water-Saturated Sand, *J. Mater. Des. Appl.*, 2007, **221**, p 21–35
8. M. Grujicic, B. Pandurangan, J.D. Summers, B.A. Cheeseman, and W.N. Roy, Application of the Modified Compaction Material Model to Soil with Various Degrees of Water Saturation, *Shock Vib.*, 2008, **15**, p 79–99
9. M. Grujicic, B. Pandurangan, I. Haque, B.A. Cheeseman, W.N. Roy, and R.R. Skaggs, A Computational Analysis of Mine-Blast Survivability of a Soft-Skin Vehicle, *Multidiscip. Model. Mater. Struct.*, 2007, **3**, p 431–460
10. M. Grujicic, B. Pandurangan, G.M. Mocko, S.T. Hung, B.A. Cheeseman, W.N. Roy, and R.R. Skaggs, A Combined Multi-Material Euler/Lagrange Computational Analysis of Blast Loading Resulting from Detonation of Buried Landmines, *Multidiscip. Model. Mater. Struct.*, 2008, **4**, p 105–124
11. M. Grujicic, B. Pandurangan, R. Qiao, B.A. Cheeseman, W.N. Roy, R.R. Skaggs, and R. Gupta, Parameterization of the Porous-Material Model for Sand with Different Levels of Water Saturation, *Soil Dyn. Earthq. Eng.*, 2008, **28**, p 20–35
12. M. Grujicic, B. Pandurangan, N. Coutris, B.A. Cheeseman, W.N. Roy, and R.R. Skaggs, Derivation and Validation of a Material Model for Clayey Sand for Use in Landmine Detonation Computational Analysis, *Multidiscip. Model. Mater. Struct.*, 2009, **5**(4), p 311–344
13. M. Grujicic, B. Pandurangan, N. Coutris, B.A. Cheeseman, W.N. Roy, and R.R. Skaggs, Computer-Simulations based Development of a High Strain-rate, Large-deformation, High-pressure Material Model for STANAG 4569 Sandy Gravel, *Soil Dyn. Earthq. Eng.*, 2008, **28**, p 1045–1062
14. M. Grujicic, B. Pandurangan, N. Coutris, B.A. Cheeseman, W.N. Roy, and R.R. Skaggs, Derivation, Parameterization and Validation of a Sandy-Clay Material Model for Use in Landmine Detonation Computational Analyses, *J. Mater. Eng. Perform.*, 2010, **10**(3), p 434–450
15. M. Grujicic, T. He, B. Pandurangan, W.C. Bell, N. Coutris, B.A. Cheeseman, W.N. Roy, and R.R. Skaggs, Development, Parameterization and Validation of a Visco-Plastic Material Model for Sand With Different Levels of Water Saturation, *J. Mater. Des. Appl.*, 2009, **223**, p 63–81
16. M. Grujicic, T. He, and B. Pandurangan, Development and Parameterization of an Equilibrium Material Model for Segmented Polyurea, *Multidiscip. Model. Mater. Struct.*, 2011 (accepted)
17. M. Grujicic, W.C. Bell, B. Pandurangan, and T. He, Blast-Wave Impact-Mitigation Capability of Polyurea When Used as Helmet Suspension-Pad Material, *Mater. Des.*, 2010, **31**, p 4050–4065
18. M. Grujicic, W.C. Bell, B. Pandurangan, and P.S. Glomski, Fluid/Structure Interaction Computational Investigation of the Blast-Wave Mitigation Efficacy of the Advanced Combat Helmet, *J. Mater. Eng. Perform.*, 2010, doi:10.1007/s11665-010-9724-z
19. M. Grujicic, B. Pandurangan, T. He, B.A. Cheeseman, C.-F. Yen, and C. L. Randow, Computational Investigation of Impact Energy Absorption Capability of Polyurea Coatings via Deformation-Induced Glass Transition, *Mater. Sci. Eng. A*, 2010, **527**(29–30), p 7741–7751
20. M. Grujicic, B. Pandurangan, A.E. King, J. Runt, J. Tarter, and G. Dillon, Multi-length Scale Modeling and Analysis of Microstructure Evolution and Mechanical Properties in Polyurea, *J. Mater. Sci.*, 2010, doi:10.1007/s10853-010-4998-y
21. M. Grujicic, B. Pandurangan, W.C. Bell, B.A. Cheeseman, C.-F. Yen, and C.L. Randow, Molecular-Level Simulations of Shock Generation and Propagation in Polyurea, *Mater. Sci. Eng. A*, 2011, doi:10.1016/j.msea.2011.01.081
22. A.V. Amirkhizi, J. Isaacs, J. McGee, and S. Nemat-Nasser, An Experimentally-Based Viscoelastic Constitutive Model for Polyurea, Including Pressure and Temperature Effects, *Philos. Mag.*, 2006, **86**, p 5847–5866
23. The Dow Chemical Company, Isonate® 143L; Modified MDI (Dow Chemical, Midland, MI, 2001)
24. Air Products Chemicals, Inc., Polyurethane Specialty Products (Air Products and Chemicals, Allentown, PA, 2003)
25. J. Yi, M.C. Boyce, G.F. Lee, and E. Balizer, Large Deformation Rate-dependent Stress-Strain Behavior of Polyurea and Polyurethanes, *Polymer*, 2006, **47**, p 319–329
26. C.M. Roland, J.N. Twigg, Y. Vu, and P.H. Mott, High Strain-Rate Mechanical Behavior of Polyurea, *Polymer*, 2007, **48**, p 574–578
27. S.S. Sarva, S. Deschanel, M.C. Boyce, and W. Chen, Stress-Strain Behavior of a Polyurea and a Polyurethane from Low to High Strain Rates, *Polymer*, 2007, **7**(48), p 2208–2213
28. H.J. Qi and M.C. Boyce, Stress-Strain Behavior of Thermoplastic Polyurethanes, *Mech. Mater.*, 2005, **37**, p 817–839
29. C. Li and J. Lua, A Hyper-Viscoelastic Constitutive Model for Polyurea, *Mater. Lett.*, 2009, **63**, p 877–880
30. R.W. Ogden, Large Deformation Isotropic Elasticity—On the Correlation of Theory and Experiment for Incompressible Rubberlike Solids, *Proc. R. Soc. Lond. A*, 1972, **326**, p 565–584
31. T. Jiao, R.J. Clifton, and S.E. Grunschel, Pressure-Sensitivity and Constitutive Modeling of an Elastomer at High Strain Rates, *16th APS Topical Conference on Shock Compression of Condensed Matter*, June 28–July 3, 2009
32. M. Grujicic, T. He, B. Pandurangan, J. Runt, J. Tarter, and G. Dillon, Development and Parameterization of a Time-invariant (Equilibrium) Material Model for Segmented Elastomeric Polyureas, *J. Mater. Des. Appl.*, 2011 (accepted)
33. E.M. Arruda and M.C. Boyce, A Three-dimensional Constitutive Model for the Large Stretch Behavior of Elastomers, *J. Mech. Phys. Solids*, 1993, **41**, p 389–412
34. T.M. El Sayed, "Constitutive Models for Polymers and Soft Biological Tissues," Ph.D. Thesis, California Institute of Technology, 2008
35. M. Ortiz and A. Molinari, Effect of Strain-Hardening and Rate Sensitivity on the Dynamic Growth of a Void in a Plastic Material, *J. Appl. Mech. Trans. ASME*, 1992, **59**(1), p 48–53
36. K. Weinberg, A. Mota, and M. Ortiz, A Variational Constitutive Model Porous Metal Plasticity, *Comput. Mech.*, 2006, **37**, p 142–152
37. ABAQUS version 6.9, User Documentation, Dessault Systems, 2007
38. W. Mock, S. Bartyczak, G. Lee, J. Fedderly, and K. Jordan, Dynamic Properties of Polyurea 1000, *Shock Compression of Condensed Matter*, American Institute for Physics, 2009, p 1241–1244
39. L. Davison, *Fundamentals of Shock-Wave Propagation in Solids*, Springer, Heidelberg, Berlin, 2008, ISBN: 978-3-540-74568-6